Microphase Separation in Super-H-Shaped Block Copolymer Colloids

G. Floudas,*,† N. Hadjichristidis,†,‡ H. Iatrou,‡ A. Avgeropoulos,‡ and T. Pakula§

Foundation for Research and Technology-HELLAS (FORTH), Institute of Electronic Structure and Laser, P.O. Box 1527, 711 10 Heraklion, Crete, Greece, Department of Chemistry, University of Athens, Panepistimiopolis, Zografou 15771, Athens, Greece, and Max-Planck Institut fur Polymerforschung, Postfach 3148, D-55021 Mainz, Germany

Received March 3, 1998; Revised Manuscript Received June 26, 1998

ABSTRACT: Block copolymers of the A_3BA_3 type with a short connector block B exhibit features known in multi-arm star polymers in addition to their block copolymer nature. We have studied the ordered state morphology and the order-to-disorder transition (ODT) in three model super H-shaped block copolymer melts of the A_3BA_3 type. From the three asymmetric nonlinear block copolymers ($0.07 < f_B < 0.35$, B is polystyrene (PS)) one is in the homogeneous disordered phase ($f_{PS} = 0.072$), another is in the ordered phase ($f_{PS} = 0.345$), and the third ($f_{PS} = 0.118$) undergoes an order-to-disorder transition in a temperature range accessible by SAXS and rheology. In the former experiment the ODT has been identified from the discontinuous changes in the peak intensity and width, whereas in the latter it has been identified by the discontinuous drop of the storage modulus. The SAXS results have shown a peculiar T dependence of the peak position q^*, which is attributed to the starlike nature of the system. TEM and SAXS identify the morphology of the $f_{PS} = 0.118$ sample as spheres organized in a body-centered-cubic (bcc) lattice with each domain consisting of about 40 connector blocks (PS), whereas in the $f_{PS} = 0.345$ sample, PS cylinders are packed in a hexagonal lattice. At some temperatures in the vicinity of the T_{ODT} two states with very different viscosities exist and large amplitude deformation and/or temperature results in a transformation from the high (state I) to the low viscosity state (state II). To identify the associated structural changes, we have compared the viscoelastic response of each state to the corresponding structural profiles. We found that the viscoelastic response in state I is controlled by the relaxation of grains whereas in state II it is controlled by the relaxation of individual domains in the absence of long range order. At low shear rates, below the grain relaxation, we identify a flow regime that is a consequence of the colloidal nature of these block copolymers.

Introduction

Linear diblock copolymers have recently received a lot of attention because of their ability to assemble into a variety of ordered structures. This ability originates from the unfavorable interactions between the two blocks and gives rise to a process known as microphase separation. The microphase separation in diblock copolymers has been studied both theoretically[1] and experimentally.[2] For a fixed value of the product χN, where χ is the interaction parameter and N is the number of segments, phase transformation can occur by changing the composition f ($=N_A/N$). Increasing asymmetry favors structures with larger curvature at the interface and in a mean-field theory (MFT) leads to a transformation from a lamellar phase to cylinders organized in a hexagonal lattice and to spheres organized in a body-centered-cubic (bcc) lattice. Novel block copolymer architectures are a promising approach to modulate various terms in the free energy balance. For example, nonlinear block copolymers such as graft copolymers (A_kB), miktoarm star copolymers (A_kB_l) and miktoarm star terpolymers (ABC) are known to be intrinsically more compatible than their linear counterparts and provide the ability to control the curvature of the interface at a fixed composition and therefore the morphology.[3] For all the above copolymers the static structure factor $S(q)$, in the disordered phase, has the following functional form:

$$\frac{N}{S(q)} = F(x, f) - 2\chi N \tag{1}$$

where $x = (qR_G)^2$ and $F(x,f)$ depend strongly on the molecular architecture. $S(q)$ has a maximum at q^* and since χ is inversely proportional to T, a plot of $S(q)^{-1}$ vs T^{-1} should give a linear dependence. In the experiments, however, such a linearity is only rarely observed. This has been attributed to the neglect of the fluctuations of the order parameter by the MFT, which when taken into account, replaces the second-order transition ($f = {}^1/_2$) at $(\chi N)_c = 10.5$ by a weak first-order transition at[4]

$$(\chi N)_{ODT} = 10.5 + \frac{41}{\bar{N}^{-1/3}} \tag{2}$$

where $\bar{N}$ is the Ginzburg parameter ($=Na^6/u^2$, a and u are the statistical segment length and volume, respectively). Furthermore, the introduction of polydispersity,[5] higher harmonics,[5,6] and conformational asymmetry effects[7] alter significantly the phase diagram of diblock copolymers. Kinetic experiments were successful in identifying the importance of fluctuations in both linear[8] and nonlinear[9,10] block copolymers. Furthermore, the $\bar{N}$ dependence of the characteristic ordering times was experimentally found[11] to be in accord with theory.[12]

The present study deals with recently synthesized[13] model nonlinear block copolymer melts of super-H shape, of the type A_3BA_3 where B is the connector (polystyrene) and A the arms (polyisoprene). These can be considered as model systems that bridge the gap

† FORTH.
‡ University of Athens.
§ Max-Planck Institut fur Polymerforschung.

S0024-9297(98)00327-1 CCC: $15.00
Published on Web 09/12/1998

between colloids and block copolymers in the sense that, in the absence of a selective solvent, they organize in a core−shell type of structure while keeping their block copolymer nature. Each block copolymer unit can be visualized as two A_3B miktoarm star copolymers with joined B blocks, but since the connector B is short compared to the arms, the molecule can also be envisioned as a six-arm polyisoprene star with a rigid core. The micellar behavior of the same samples in a selective solvent has recently been reported.[14] Here we identify the ordered state morphology by SAXS and TEM and study the order-to-disorder transition in these asymmetric super-H-shaped copolymer melts. Both techniques provide the order-to-disorder transition temperature (T_{ODT}) and address the importance of fluctuations in such complex nonlinear block copolymers. With rheology we identify (i) the relaxation of coherent grains, (ii) the destruction of grains under large amplitude deformation and/or temperature and the relaxation of individual domains, and (iii) the flow-regime characteristic of the colloidal nature of the block copolymers.

Experimental Section

Samples. The basic reactions used for the synthesis of the super-H-shaped copolymers of the $(PI)_3(PS)(PI)_3$ type, where PI is polyisoprene and PS is protonated (PS-h_8) or deuterated (PS-d_8) polystyrene, are schematically the following:

$$\text{naphthalene} + \text{Na} \rightarrow \text{sodium naphthalenide (I)}$$

$$\text{(I)} + \text{St} \rightarrow \text{Na(PS)Na (II)}$$

$$\text{(II)} + \text{excess } SiCl_4 \rightarrow Cl_3Si(PS)SiCl_3\ \text{(III)} + 2\text{NaCl} + SiCl_4\uparrow$$

$$\text{(III)} + \text{excess PILi} \rightarrow (PI)_3(PS)(PI)_3 + 6\text{LiCl} + \text{PI}\downarrow\ \text{(SH-shaped copolymer)}$$

where St is protonated or deuterated styrene. The preparation of the initiator and of the difunctional PS connector has already been described in previous publications.[14,15] The linking reaction of the living difunctional connector with the tetrachlorosilane was performed as described elsewhere by Iatrou and Hadjichristidis.[16,17] A small aliquot (∼1 g) of the arms and the connector was always removed for characterization. The SEC chromatogram of the hexafunctional macromolecular linking agent (III) was almost indistinguishable from the parent material (II). A typical example is given in Figure 1 where the raw product along with the fractionated SH copolymer are shown. Fractionation of the super H-shaped copolymers was performed by addition of methanol to a 0.1−0.5% solution in toluene. After the fractionation, all the side products were eliminated, and the SEC traces indicated higher than 99% purity for the SH-shaped copolymers. SEC experiments were carried out at 25 °C using a Waters 150C instrument. Four μ-Styragel columns with a continuous porosity range from 10^5 to 500 Å were used together with one ultra-Styragel column of continuous porosity. Tetrahydrofuran (THF) was the carrier solvent at a flow rate of 1 mL/min. SEC experiments were also performed with a refractive index and UV detector in series for the analysis of the polymer composition over the elution peak.

The weight-average molecular weight M_w(SH) of the SH copolymer was measured at 25 °C with a Chromatix KMX-6 low-angle laser photometer in THF operating at 633 nm. The refractive index increment dn/dc was measured under the same conditions with a Chromatix KMX-16 refractometer calibrated with aqueous NaCl solutions. The number-average molecular weights M_n were determined with a Wescan model 230 membrane osmometer (MO) at 37 °C and in a few cases ($M_n \leq 0.84 \times 10^4$) with a Wescan Model 233 vapor pressure osmometer (VPO) at 50 °C. Toluene, distilled over CaH_2, was used as solvent.

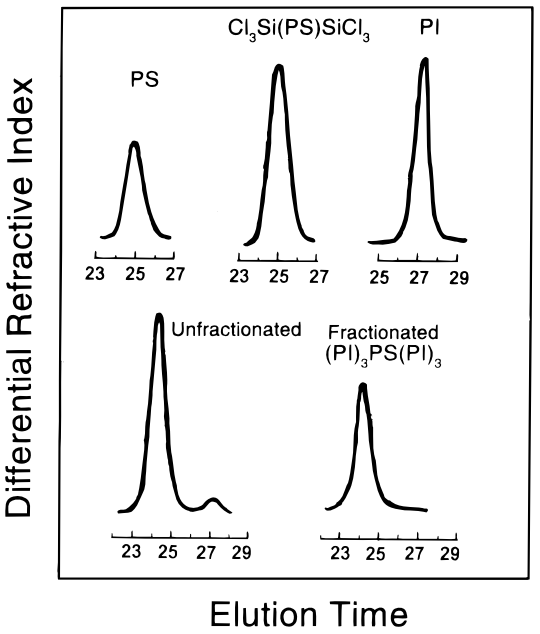

Figure 1. SEC chromatograms of the SH10-20 block copolymer.

The characteristics of the precursors and the fractionated SH block copolymers are given in Table 1. There are several factors that show the high degree of homogeneity in molecular weight and composition for the super-H-shaped copolymers: the good agreement between (a) the values found by osmometry and the calculated ones from M_n(SH) = M_n(con) + 6M_n(arm), (b) the apparent molecular weight obtained by low-angle laser light scattering (LALLS) and the M_w calculated from the M_n(SH) and the polydispersity index, and (c) the PS content of the SH copolymers calculated from the M_n of the connector and the arms and that found by UV (deuterated samples) and NMR (protonated samples) spectroscopy. Table 2 gives the composition and phase state (see below) of the copolymers.

Small-Angle X-ray Scattering. A Kratky compact camera (Anton Paar KG) equipped with a one-dimensional position-sensitive detector (M. Braun) was used for the SAXS experiment. The Ni-filtered Cu Kα radiation (λ = 0.154 nm) was used from a Siemens generator operating at 35 kV and 30 mA. Measurements of 1 h long were made at intervals of 5 K within the range 303−423 K, and the stability was better than ±0.2 K. Changes between successive temperatures were completed within ∼5 min, and a 30 min waiting time was preset for equilibration. The smeared intensity data were collected in a multichannel analyzer and transferred to a Vax computer for further analysis. Smeared intensities were subsequently corrected for absorption, background scattering, and slit-length smearing. Primary beam intensities were determined, in absolute units, by using the moving slit method. Additionally, a 18-kW rotating anode X-ray source (Rigaku) with a pinhole collimation and a two-dimensional detector (Siemens) with 512 × 512 pixels was used for a sample that was sheared with large amplitude oscillations.

Transmission Electron Microscopy. A Zeiss EM 902 electron microscope was used on ultrathin sections of the SH20-20 copolymer. Prior to sectioning at −30 °C, the sample was exposed to OsO_4 vapor for 1 day. Micrographs were recorded on a Kodak FGRP 35 mm film. For the SH3 copolymer a film was cast from a ∼5% w/v toluene solution. Microtomed sections (50 nm thick) were stained with OsO_4 for 1 h.

Rheology. A Rheometric scientific dynamic stress rheometer (DSR) together with an advanced rheometric expansion system (ARES) equipped with a force-rebalanced transducer were used for most of the studies. Both oscillatory shear and

Table 1. Molecular Characteristics of the Super-H-Shaped Block Copolymers

		$10^{-4}M_n$[a]					PS (or PS-d_8) (w %)	
sample	chemical formula	connector	arm	SH	$10^{-4}M_w$ (SH)[b]	M_w/M_n[c]	M_n[e]	UV
SH10-20	$(PI)_3(PS\text{-}d_8)(PI)_3$	0.84[d]	1.56	10.8	10.9	1.04	8.2	8.5
SH20-20	$(PI)_3(PS\text{-}d_8)(PI)_3$	1.68	1.79	12.0	12.8	1.03	13.5	14
SH3	$(PI)_3(PS)(PI)_3$	10.9	2.94	29.0	30.8	1.07	38	37[f]

[a] MO in toluene at 37 °C. [b] LALLS in THF at 25 °C. [c] SEC in THF at 25 °C. [d] VPO in toluene at 50 °C. [e] Calculated from the M_n of connector and arms. [f] By NMR.

Table 2. Composition and Phase State of the Super-H-Shaped Block Copolymers

sample	$N_{n,PS}$*[a]	$N_{n,PI}$*	f_{PS}[b]	N[c]	T_{ODT} (K)	$(\chi N)_{ODT}$[d]
SH10-20	93	1205	0.072	4100	disordered	
SH20-20	185	1383	0.118	4960	389	103
SH3	1197	2271	0.345	10965	ordered	

[a] $N_{n,PS}^* = N_{n,PS}(\rho_I^*/\rho_S^*)^{1/2}$, where $N_{n,i}$ are the degrees of polymerization for each block and ρ_I^* and ρ_S^* are the molar densities. [b] Calculated from $f = N_{n,PS}^*/N_{n,total}$. [c] Based on $a = 6.35$ Å and $u = 144$ Å^3. [d] Based on $\chi = 0.04 + (10/T)$.

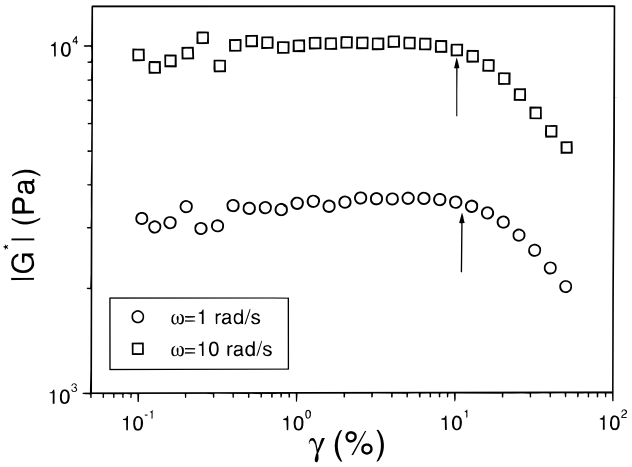

Figure 2. Strain dependence of the magnitude of the complex shear modulus G^* for the super-H-shaped SH20-20 block copolymer at $T = 373$ K and at two frequencies, as indicated. Arrows separate the linear from the nonlinear viscoelastic range.

steady shear experiments have been performed. In the first experiment the strain amplitude dependence of the complex shear modulus G^* was investigated. The strain dependence of the magnitude of G^* for the sample SH20-20 is shown in Figure 2 at $T = 373$ K for strain amplitudes in the range 0.1−100% for two frequencies. The arrows separate the linear from the nonlinear viscoelastic range and strain amplitudes well within the linear viscoelastic range (typically about 1%) were used for the remaining study. Such experiments involved isochronal temperature scans at $\omega = 1$ rad/s, isothermal frequency scans, and isochronal/isothermal time scans at selected temperatures below the order−disorder transition. Furthermore, shear creep compliance and recovery compliance measurements were made for one of the samples (SH20-20). The only experiment with a strain amplitude corresponding to the nonlinear viscoelastic range was made to induce orientational order in the material with large amplitude oscillation ($T = 375$ K, $\omega = 1$ rad/s, and strain amplitude = 20%). The sample was subsequently quenched to ambient temperature and examined with the 2-dimensional detector.

Results and Discussion

Ordered State Morphology. To establish the ordered state morphology, we performed SAXS and TEM on annealed SH20-20 samples and the results are shown, respectively, in Figures 3 and 4. In Figure 3 the SAXS spectrum at $T = 353$ K is shown and displays

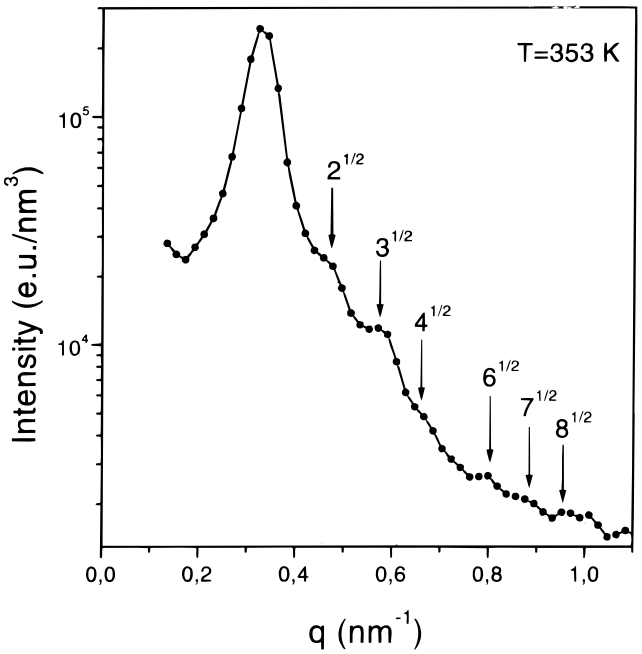

Figure 3. SAXS spectrum of the SH20-20 at $T = 353$ K showing the formation of a spherical microstructure. The arrows indicate the Bragg reflections coresponding to a bcc lattice

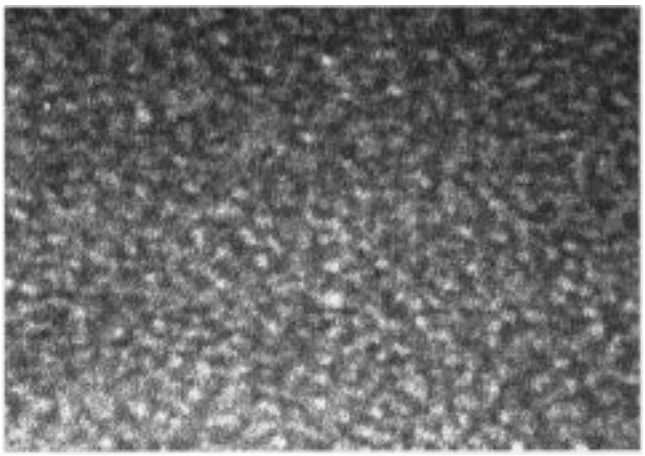

Figure 4. TEM of the sample SH20-20 showing spherical domains of the minority phase (light phase) in the matrix of PI (dark phase).

a main peak at q^* followed by higher order peaks at positions $2^{1/2}$, $3^{1/2}$, $4^{1/2}$, and $6^{1/2}$ and more weak reflections at $7^{1/2}$ and $8^{1/2}$ relative to the main peak. These reflections are characteristic of spheres in a bcc lattice; however, the absence of the weak $7^{1/2}$ reflection would result in an sc lattice. Given the known phase diagrams from diblock copolymers, a bcc structure is certainly a more likely scenario. The size of the minority phase forming the core can be estimated from the Bragg spacing and simple geometrical considerations. For a

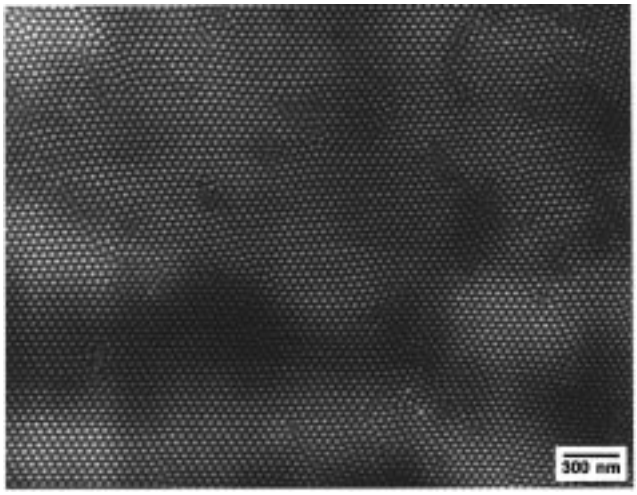

Figure 5. TEM of the sample SH3 showing a nearly axial projection of hexagonally packed PS cylinders in the PI matrix.

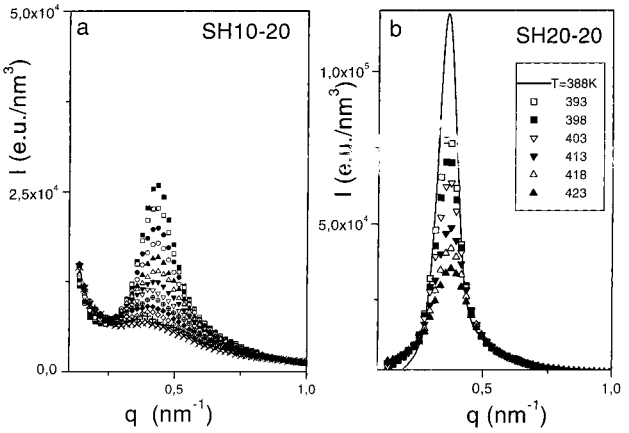

Figure 6. (a) SAXS profiles for SH10-20 shown for temperatures in the range $308 \leq T \leq 368$ K in steps of 5 K. (b) SAXS profiles for the SH20-20 sample shown for temperatures in the range $388 \leq T \leq 423$ K. At temperatures below 389 K two additional reflections appear indicating the formation of a structure with cubic symmetry.

bcc lattice the PS radius is $R_{PS} = (f_{PS} d_o^3/3^{1/2}\pi)^{1/3}$, where d_o is the nearest neighbor distance between spheres ($d_o = d(3/2)^{1/2}$) and $d = 2\pi/q^*$, resulting in $R_{PS} = 6.4$ nm. On the basis of the volume of a PS chain, we find that there are about 40 PS connectors per micelle. Thus, each micelle has a shell of about 240 PI chains, making a great resemblance to multiarm stars.

The ordered state morphology of SH20-20 was also studied by TEM, and the micrograph of Figure 4 exhibits spherical domains of the minority phase with a mean spacing that corresponds well to the one extracted from SAXS. The morphology of the SH3 sample was also studied with TEM, and the result is shown in Figure 5. The micrograph shows a nearly axial projection of hexagonally packed PS cylinders in the PI matrix.

Order-to-Disorder Transition and Disordered State Structure Factor. The T dependence of the structure factor has been studied next. The desmeared SAXS profiles for two of the samples are shown in Figure 6. The profile for the third copolymer (SH3) is not shown since the intense peak has moved to smaller q values that are beyond our experimental resolution. The spectra in Figure 6 show three basic features: (i) a peak at q^* whose intensity and position depend on T, (ii) an upturn at small q, and (iii) a background contribution. The first feature contains most of the information about the process of microphase separation. The upturn at small q's is related mainly to long-range fluctuations. These fluctuations are not solely of the same origin as the concentration fluctuations responsible for the peak at q^*. This feature is common for all glass-forming liquids and homopolymers and is more pronounced at lower temperatures. Fischer has shown[18] that the intensity measured at ultralow q's ($I(q \rightarrow 0)$) is not proportional to the isothermal compressibility and that the excess intensity is caused by long-range spatial heterogeneities in density. In multicomponent systems the excess intensity at low q's contains contributions from the excess density and the concentration fluctuations, but the relative contribution of the two is not known. As for the third process, i.e., the background contribution at higher q's, we have shown in our earlier work[19] that it is caused again by both: thermal density and concentration fluctuations. The former are calculated from the measured isothermal compressibility β_T-(T) as

$$I_d(q=0) = \bar{n}^2 k_B T \beta_T \tag{3}$$

where $\bar{n}$ is the average electron density. The intensity $I(0)$, which is calculated at every temperature, is now subtracted from the measured intensities. This procedure gives the spectrum of the concentration fluctuations alone for q's higher than the low-q region. The latter are given by

$$I_c = \Delta n^2 V S_c(q) \tag{4}$$

where Δn ($=n_{PS} - n_{PI}$) is the difference in the electron densities of PS and PI, V is the volume of a chain, and $S_c(q)$ is the static structure factor for concentration fluctuations. Increasing T has opposite effects on the density and concentration fluctuations: the former increase whereas the latter decrease with T. This makes the subtraction of the density fluctuations necessary at least at high T. The decrease and broadening of the SAXS peak intensity (Figure 6a) implies considerable mixing between PS and PI segments with increasing T. The peak, however, persists at q^* even at the highest temperature (well within the disordered phase) due to the correlation hole effect.[1,20] The SAXS spectra for the two samples (Figure 6) are distinctly different with respect to their temperature dependence. For the SH10-20, there is a continuous decrease of the peak intensity with increasing T (disordered phase). Alternatively, for SH20-20 there is a discontinuous drop of the peak intensity at $T \approx 389$ K (order−disorder transition). Moreover, at $T < 389$ K additional reflections develop at higher q's (Figure 3), indicating the formation of the bcc structure.

The peak parameters, extracted from a Lorentzian fit, are plotted in Figure 7 as a function of temperature for SH10-20 and SH20-20. For SH20-20, the peak intensity and width are discontinuous functions of T (vertical line in Figure 7 indicates the T_{ODT}), but q^* varies linearly with inverse temperature.[21] Notice the curvature of the data in the plot $I(q^*)^{-1}$ vs T^{-1} for SH20-20 at $T > T_{ODT}$ and for SH10-20, which is well within the homogeneous phase. Such nonlinear dependencies contradict the mean-field predictions (eq1) and demonstrate the importance of fluctuations. A new feature is the T

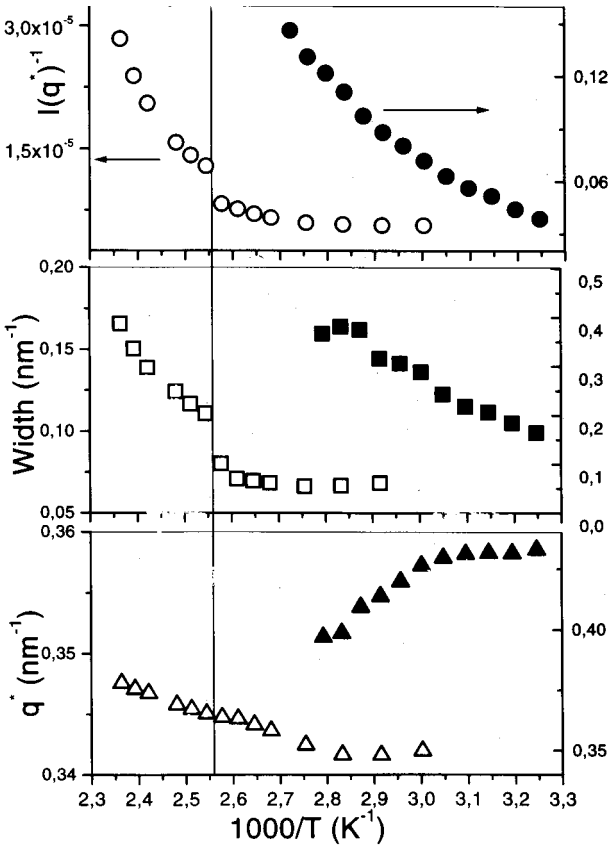

Figure 7. Comparison of the peak parameters (inverse peak intensity, peak position and width) for SH10-20 (filled symbols) and SH20-20 (open symbols) plotted vs inverse temperature. The vertical line indicates the T_{ODT} for the latter.

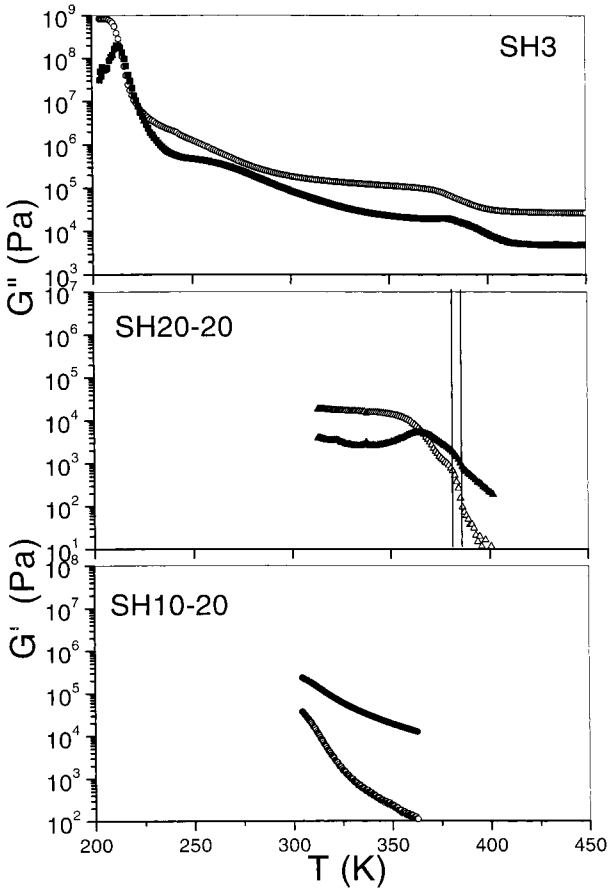

Figure 8. Isochronal measurements of the storage and loss moduli at 1 rad/s for the three super-H-shaped SI copolymers. The vertical lines for SH20-20 indicate the T_{ODT}. Measurements have been made with a low strain amplitude.

dependence of q^* for SH10-20, which decreases with increasing temperature. The origin of this T dependence can be discussed in the context of the star shape of this very asymmetric block copolymer ($f_{PS} = 0.072$). At T much above the T_{ODT}, the system is in the homogeneous state and the peak in the structure factor reflects mainly the scattering due to single PS connectors (correlation hole scattering). As the temperature is reduced, some of the PS connectors can assemble into domains without exhibiting long range order. This process of preseparation creates higher contrast, but there is only a limited number of PS connectors that can be incorporated into the core due to the thermodynamic force favoring mixing ($T > T_{ODT}$). There is a delicate balance between chains in the core−shell arrangement and completely mixed chains, and upon further reduction of T, the creation of new core−shell structures at some intermediate distances from the primary structures becomes favorable. This results in the observed decrease of the characteristic distance between the cores and thus in the observed increase of q^*. By a further decrease in T these core−shell structures are stabilized both in size and in aggregation numbers and result progressively in the microphase separation. At this final state the PI arms become extended, thus giving rise to the increase in $q^*(T)$ found in SH20-20. It is this pre-ordering mechanism (without long-range order) followed by the microphase separation (lattice formation) that enhances the resemblance of these block copolymers with multiarm star colloids.

Rheology. It is known[8] that isochronal temperature measurements performed by heating the specimen can provide (together with the kinetic studies) the order−disorder transition in block copolymers. We have shown earlier[22] that the process of dissolution occurs on a much faster time scale than the ordering process, and this is the main reason that the isochronal scans are made by heating. The result of such scans are shown in Figure 8 for the three copolymers at $\omega = 1$ rad/s. The absolute values and the temperature dependencies of the storage (G') and loss (G'') moduli are distinctly different for the three samples: sample SH3 undergoes multiple relaxations within the ordered phase, which correspond, from low to high T, to the PI segmental relaxation, the PI block relaxation, and the PS segmental relaxation. However, even at the highest measurement temperature the samples exhibit a rubber-like response with $G' > G''$ (ordered phase). In contrast, for SH10-20, $G' < G''$ (disordered phase) over the whole temperature range above room temperature and this "liquidlike" rheological response is in excellent agreement with the "liquidlike" structure factor from SAXS (Figure 6a). Alternatively, sample SH20-20 undergoes an order-to-disorder transition at 385 K, that is, at about 4 K lower temperature than the SAXS result (Figure 6b). The reason for this difference, which is well beyond the T resolution in both experiments, can be related to the nonequilibrium state of the system below the ideal order-to-disorder transition temperature. We have shown recently[23] that there exists an equilibrium order-to-disorder transition temperature in analogy to the equilibrium melting temperature in semicrystalline polymers. Below this temperature only apparent transition temperatures can be defined.

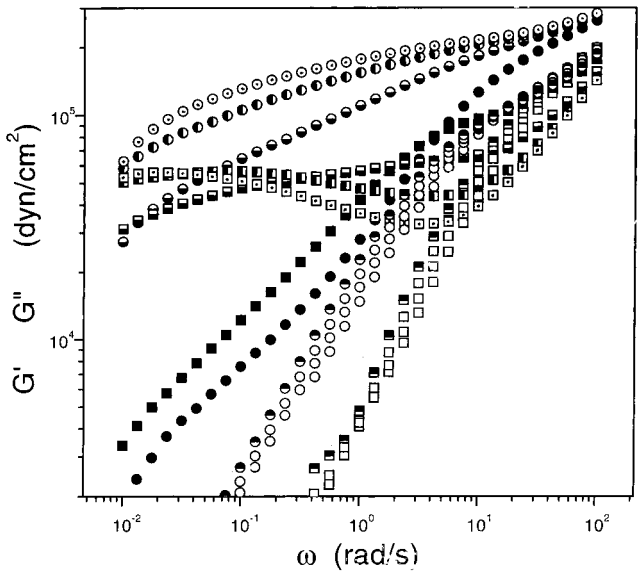

Figure 9. Frequency dependence of G' (circles) and G'' (squares) of sample SH20-20, at different temperatures below and above the ODT. Only data at some selected temperatures are shown: (○) $T = 372$, (◐) $T = 375$, (◒) $T = 378$, (●) $T = 382$, and (◓) $T = 385$ K. Notice the maximum in G'' that develops for some temperatures below the T_{ODT}.

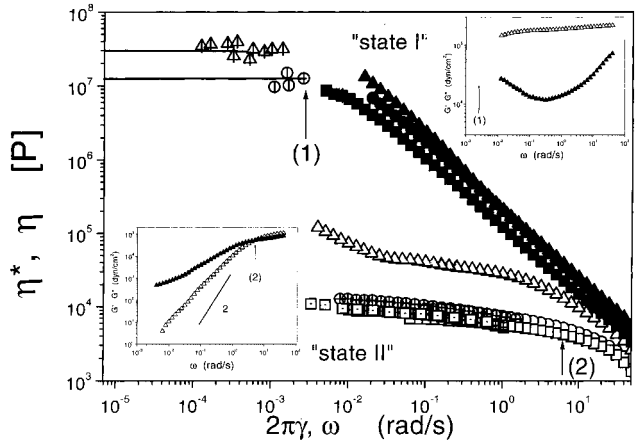

Figure 10. Viscosity of SH20-20 at different temperatures below the order−disorder transition: (squares) $T = 377$ K; (circles) $T = 373$ K; (triangles) $T = 368$ K. Filled and open symbols correspond to states I and II, respectively (see text). Viscosities are obtained by three independent experiments: (i) dynamic frequency sweeps, (ii) steady stress sweeps (half-filled symbols), and (iii) steady rate sweeps (dotted symbols). The upper and lower insets show, respectively, the frequency dependent moduli for the states I and II. The characteristic relaxation times (see text) are indicated with arrows.

In the next experiment we performed isothermal frequency sweeps in the range from 10^{-2} to 10^{2} rad/s with small strain amplitude (usually about 1%) and the data are shown in Figure 9 for SH20-20. The linear viscoelastic properties of microphase-separated block copolymers have been the subject of recent theoretical studies. In the study by Rubinstein and Obukhov,[24] both microscopic and mesoscopic mechanisms have been invoked, which were attributed, respectively, to the dispersion in the number of entanglements of a chain with the opposite brush (high-frequency response) and to the collective diffusion of copolymer chains along the interface. The latter mechanism is controlled by defects in lamellar orientation and contributes to the low-frequency side, which is of interest to us. For the disordered lamellar mesophase they predict $G'(\omega) \approx G''(\omega) \approx \omega^{1/2}$, whereas for the cylindrical mesophase $G'(\omega) \approx G''(\omega) \approx \omega^{1/4}$. On the other hand, Kawasaki and Onuki[25] reached the same conclusion through a completely different approach: they proposed that overdamped second-sound modes in an orientationally disordered lamellar phase could result in a complex shear modulus proportional to $(i\omega)^{1/2}$. A pertinent feature of the moduli shown in Figure 9, which is not accounted for by the above theoretical studies, is that for some temperatures in the ordered phase the loss moduli exhibit a maximum, which signifies a new characteristic frequency for the relaxation of the ordered phase. We attribute the maximum in $G''(\omega)$ to the grain relaxation (see below). Such a dependence of G'' on frequency has been reported for other bicontinuous ($I\alpha\bar{3}d$) and spherical ($Im3m$) morphologies.[26] Similarly, in the asymmetric miktoarm stars $(PS)_2(PI)_2$,[27] there was an upturn of G'' at low frequencies, which was found to depend on the annealing history and therefore the coherence of grains. Earlier investigations on a linear and nearly symmetric PEP−PEE copolymer[28] indicated the presence of long-time relaxation modes relaxing, however, at very low shear rates, which were not accessible by the experiment. The reason for the accelerated grain relaxation in the present system is the higher mobility ($f_{PS} = 0.12$). As we will see below, the situation shown in Figure 9 is only one possibility (state I). Subjecting the system to large amplitude deformation (oscillatory or steady) results in a different behavior (state II).

This is shown in Figure 10 where we plot the viscosity for the two phases from three different experiments: (i) dynamic frequency sweeps ($\eta^*(\omega)$) in the range $4 \times 10^{-3} < \omega < 10^{2}$ rad/s, with strain amplitude below 2%, (ii) steady stress sweeps ($\eta(\dot{\gamma})$), and (iii) steady rate sweeps ($\eta(\dot{\gamma})$). The results are shown for three temperatures below the ODT: 368 (triangles), 373 (circles), and 377 K (squares). The results show a drastic change of the viscoelastic properties of the system by a large amplitude oscillatory deformation. In state I, where a small deformation is applied, there is nearly a plateau in G' with a small drop at the low-frequency side, suggestive of a relaxation process at low frequencies (arrow (1) in the upper inset of Figure 10). The behavior after deformation (state II) indicates a flow of the system with a much shorter relaxation time. The latter can be defined by the crossing of G' and G'' (arrow (2) in the lower inset of Figure 10). Furthermore, the viscosity of state I reaches a Newtonian plateau at low shear rates. The empirical Cox−Merz rule, $\eta^*(\omega) = \eta(\dot{\gamma})$, holds for the two lowest temperatures shown and only approximately at 377 K. The arrow (1) in the viscosity data of Figure 10 gives an approximate shear rate below which the zero shear viscosity is obtained. It is the first time, to our knowledge, that a Newtonian viscosity plateau is obtained in a microphase-separated block copolymer. The reason is that the present system behaves like multiarm stars, which are known to flow at low frequencies.[29]

In an attempt to explain the complex viscoelastic properties of the system we have considered different possibilities and used the information on the structure from the SAXS and TEM experiments. The structure of the SH20-20 copolymer has been identified as spherical microdomains (bcc) formed by a number of copolymers. As discussed earlier, due to the short connector length, this structure resembles multiarm starts that

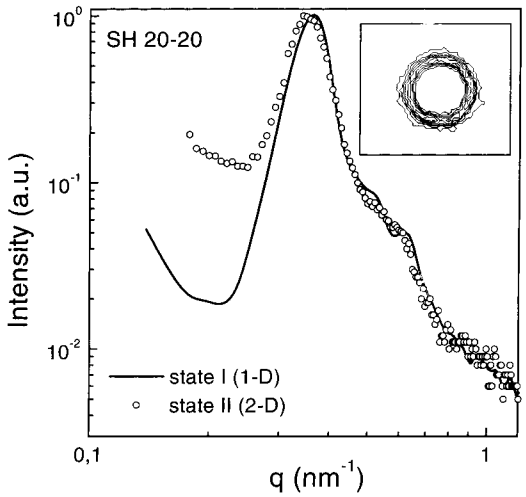

Figure 11. Comparison of the scattering profiles corresponding to states I (solid line) and II (circles). The profile of state I is obtained with a one-dimensional detector at 378 K. State II is produced by applying a large amplitude deformation at 375 K. The sample is quenched and measured with a 2-D detector at 300 K (the edge view is shown). The inset gives the 2-D pattern, which shows the absence of macroscopic orientation.

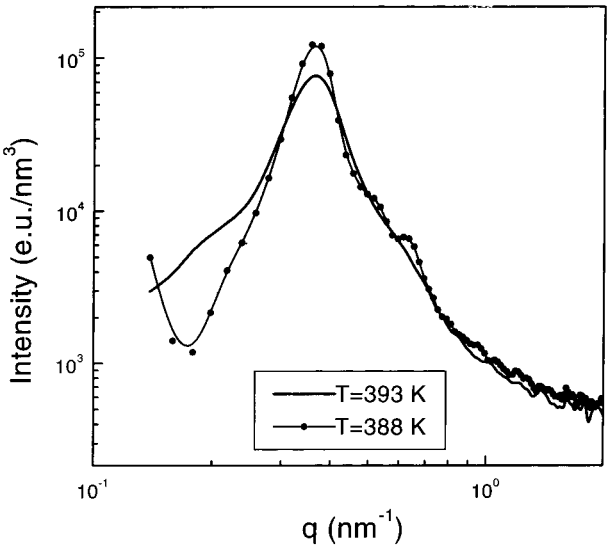

Figure 12. Comparison of the SAXS profiles of SH20-20 at two temperatures, as indicated. Notice the resemblance of the spectrum at 393 K, which is above the ODT, with the one of Figure 11 corresponding to state II obtained by large amplitude deformation at T below the ODT.

have very long relaxation times. On the basis of the SAXS (Figure 3) and TEM (Figure 4) results, the corresponding structure to this state (state I) consists of spherical microdomains with a uniform lattice order and the relaxation of this state is indicated with (1) and is assigned to the relaxation of *grains*. Next, we subject the grain structure to large amplitude oscillation. For the resulting state II there are two possibilities: state II can be produced (i) by the formation of a macrolattice or (ii) by a destruction of the initial lattice order and consequently a reduction of the relaxation times to those characteristic for a single microdomain in a state with liquidlike order. The two cases (i) and (ii) imply specific structural changes in the system. The formation of a macrodomain should be detectable by a two-dimensional scattering pattern, which will indicate a preferential orientation of the lattice in the deformed sample. In the second case there is no reason to expect any detectable orientation, but some effects should be observed in the scattering peak intensity. It is evident that the comparison between the scattering patterns of states I and II is crucial for the interpretation of the observed viscoleastic response.

This comparison is made in Figure 11 where we plot two scattering profiles of SH20-20: the first (solid line) is measured at 378 K from a sample corresponding to state I and the second (circles) to a sample subjected to large amplitude deformation at 375 K, which was subsequently quenched to 300 K and measured with the 2-D detector (only the edge view is shown) (state II). The 2-D pattern for the sample in state II is shown as an inset. There is nearly no change in the main peak position, and no preferential orientation is detected in state II. This result implies that the initial ordered structure (state I) is destroyed by the large amplitude oscillatory deformation (state II). The relaxation in the ordered state I is too slow to appear within the experimental window and results in the plateau of the modulus. In state II, the relaxation of the system is controlled by the relaxation of individual domains that have much shorter relaxation times and appear as a crossing of G' and G'' at higher frequencies. In the latter state the destruction of the lattice order is not complete and there is still some liquidlike order, as indicated by the presence of higher order maxima in the scattering profile, however, with more weak intensity and broader than in state I. The viscoelastic behavior corresponding to state II indicates also a small contribution of longer relaxation processes (turn up in G'' at low frequencies). This probably means that the destruction of the lattice order takes place mainly at grain boundaries and the system can be regarded as a dispersion of grains possessing liquidlike order.[30]

Large deformation is only one possibility of producing state II. Another possibility is by changing temperature. At T just above the ODT, the viscoelastic properties of the system revealed that flow of spheres with liquidlike order is possible. To illustrate this we are comparing the structure factors at two temperatures below and above the transition, in Figure 12. The spectra at $T > T_{ODT}$ show a broadened main peak at q^* followed by a very broad shoulder at higher q, in the vicinity of the higher order peaks of the bcc structure. Notice the similarity of the spectrum at 393 K (above the ODT) with the spectrum of Figure 11 corresponding to state II, which was obtained by applying large amplitude deformation to the sample below the ODT. The similarity of the two scattering profiles clearly demonstrates that the profile at 393 K corresponds to a liquidlike arrangement of PS spheres (state II). We have shown that this state of order (or disorder) can be obtained by means of deformation or simply by increasing temperature.

In a separate experiment we have performed shear creep and recovery measurements on state II, aiming to extract the long characteristic time. The experiments consistent of 2×10^4 s of creep for the three temperatures (T = 369, 372, and 375 K). The result for the recoverable compliance J_r (not shown here) revealed very long times characterizing state II. This behavior for J_r has also been encountered in symmetric PEP−PEE diblock copolymers.[28] Last, the ordering kinetics in these complex block copolymers as compared to their

linear counterparts have been investigated and will be reported in the future.

Conclusion

Super-H-shaped block copolymers with a short connector block resemble multiarm stars and behave like block copolymer colloids in the absence of solvent. We have shown that when the volume fraction of the connector block is about 0.12, the structure consists of spheres organized in a bcc lattice with each domain consisting of about 40 connector blocks. This results in the formation of the core−shell type of morphology even in the disordered state with approximately 240 PI blocks forming the shell. With decreasing temperature these colloidal "particles" organize in a lattice, giving rise to the measured (by SAXS) changes of the structure factor. From the T dependence of the SAXS profiles, deviations from the mean-field behavior have been identified at temperatures well above the T_{ODT}. Rheology has been used in parallel with SAXS. We find a state where the PS spheres are arranged with a liquid-like order by applying large amplitude deformation in the ordered state or by increasing temperature just above the transition. Furthermore, we identify a flow regime in these ordered block copolymers, which is expected from their colloidal nature.

Acknowledgment. G.F. acknowledges the support of the Alexander von Humboldt Foundation for a grant (FOKOOP). We thank Dr. G. Lieser from the MPI-P for the TEM study.

References and Notes

(1) Leibler, L. *Macromolecules* **1980**, *13*, 1602.
(2) See, for example: Bates, F. S.; Fredrickson, G. H. *Annu. Rev. Phys. Chem.* **1990**, *41*, 525.
(3) Milner, S. T. *Macromolecules* **1994**, *27*, 2333.
(4) Fredrickson, G. H.; Helfand, E. *J. Chem. Phys.* **1987**, *87*, 697.
(5) Erukhimovich, I. Ya.; Dobrynin, A. V. *Macromol. Symp.* **1994**, *81*, 253.
(6) Olvera de la Cruz, M.; Mayes, A. M.; Swift, B. W. *Macromolecules* **1992**, *25*, 944.
(7) Vavasour, J. D.; Whitemore, M. D. *Macromolecules* **1993**, *26*, 7070.
(8) (a) Rosedale, J. H.; Bates, F. S. *Macromolecules* **1990**, *23*, 2329. (b) Floudas, G.; Pakula, T.; Fischer, E. W.; Hadjichristidis, N.; Pispas, S. *Acta Polym.* **1994**, *45*, 176. (c) Stühn, B.; Vilesov, A.; Zachmann, H. G. *Macromolecules* **1994**, *27*, 3560. (d) Adams, J. L.; Quiram, D. J.; Graessley, W. W.; Register, R. A.; Marchand, G. R. *Macromolecules* **1996**, *29*, 2929. (e) Hashimoto, T.; Sakamoto, N. *Macromolecules* **1995**, *28*, 4779.
(9) Floudas, G.; Hadjichristidis, N.; Iatrou, H.; Pakula, T.; Fischer, E. W. *Macromolecules* **1994**, *27*, 7735.
(10) Floudas, G.; Pispas, S.; Hadjichristidis, N.; Pakula, T.; Erukhimovich, I. *Macromolecules* **1996**, *29*, 4142.
(11) Floudas, G.; Vlassopoulos, D.; Pitsikalis, M.; Hadjichristidis, N.; Stamm, M. *J. Chem. Phys.* **1996**, *104*, 2083.
(12) Fredrickson, G. H.; Binder, K. *J. Chem. Phys.* **1989**, *91*, 7265.
(13) Iatrou, H.; Avgeropoulos, A.; Hadjichristidis, N. *Macromolecules* **1994**, *27*, 6232.
(14) Iatrou, H.; Willner, L.; Hadjichristidis, N.; Halperin, A.; Richter, D. *Macromolecules* **1996**, *29*, 581.
(15) Roovers, J.; Toporowski, P. *Macromolecules* **1981**, *14*, 1174.
(16) Iatrou, H.; Hadjichristidis, N. *Macromolecules* **1992**, *25*, 4649.
(17) Iatrou, H.; Hadjichristidis, N. *Macromolecules* **1993**, *26*, 2479.
(18) Fischer, E. W. *Physica A* **1993**, *A201*, 183.
(19) Floudas, G.; Vogt, S.; Pakula, T.; Fischer, E. W. *Macromolecules* **1993**, *26*, 7210.
(20) de Gennes, P.-G. In *Scaling Concepts in Polymer Physics*; Cornell University Press: Ithaca, NY, 1979.
(21) A linear dependence of Q^* on T^{-1} is not the rule in block copolymers: in asymmetric linear diblock copolymers[10] and in asymmetric graft copolymers of the A_2B type[9] a discontinuous change of Q^* towards smaller values has been reported with increasing T, in the vicinity of the T_{ODT}.
(22) Floudas, G.; Fytas, G.; Hadjichristidis, N.; Pitsikalis, M. *Macromolecules* **1995**, *28*, 2359.
(23) Floudas, G.; Pakula, T.; Velis, G.; Sioula, S.; Hadjichristidis, N. *J. Chem. Phys.* **1998**, *108*, 6498.
(24) Rubinstein, M.; Obukhov, S. P. *Macromolecules* **1993**, *26*, 1740.
(25) Kawasaki, K.; Onuki, A. *Phys. Rev. A* **1990**, *42*, 3664.
(26) Zhao, J.; Majumdar, B.; Schulz, M. F.; Bates, F. S.; Almdal, K.; Mortensen, K.; Hajduk, D. A.; Gruner, S. M. *Macromolecules* **1996**, *29*, 1204.
(27) Johnson, J. M.; Allgaier, J. B.; Wright, S. J.; Young, R. N.; Buzza, M.; McLeish, T. C. B. *J. Chem. Soc., Faraday Trans.* **1995**, *91*, 2403.
(28) Koppi, K. A.; Tirrell, M.; Bates, F. S.; Almdal, K.; Colby, R. H. *J. Phys. II France* **1992**, *2*, 1941.
(29) Pakula, T. *Macromolecules* **1997**, *30*, 8463.
(30) It is known [Bruinsma, R.; Rabin, Y. *Phys. Rev. A* **1992**, *45*, 994] that shear flow can lead to enhancement or suppression of concentration fluctuations when the shear rate approaches the reciprocal of the microstructural relaxation time.

MA9803279